JAERI-M
9181

IMPURITY STATUS OF DEE-SHAPED DISCHARGES IN DOUBLET III WITH INCONEL WALL AND LIMITERS

- WITH AND WITHOUT TITANIUM GETTERING -

(Doublet-III Experimental Report, 5)

November 1980

Noboru FUJISAWA, Masayuki NAGAMI, Hideaki YOKOMIZO,
Michiya SHIMADA, Shigeru KONOSHIMA, Shogo SEKI,
Toru SUGAWARA*, Yoshihiro OHARA, Kimihiro IOKI,**
Gary L. JAHNS,*** Neil H. BROOKS,*** Richard GROEBNER,***
Akio KITSUNEZAKI

日本原子力研究所
Japan Atomic Energy Research Institute

JAERI-M 9181

Impurity Status of Dee-shaped Discharges in Doublet III with Inconel Wall and Limiters - with and without Titanium Gettering - (Doublet III Experimental Report, 5)

Noboru FUJISAWA, Masayuki NAGAMI, Hideaki YOKOMIZO,
Michiya SHIMADA, Shigeru KONOSHIMA, Shogo SEKI,
Tohru SUGAWARA*, Yoshihiro OHARA, Kimihiro IOKI**,
Gary L. JAHNS***, Neil H. BROOKS***, Richard GROEBNER***,
Akio KITSUNEZAKI

Division of large Tokamak Development,
Tokai Research Establishment, JAERI

(Received October 16, 1980)

Dee-shaped discharges in the Doublet III device have the folloing plasma parameters: maximum discharge current 1.0 MA, maximum mean density 1.0×10^{14} cm^{-3}, elongation 1.0-1.6. The dominant impurities are oxygen and nickel, which are the major constituents of the Inconel limiters and vessel wall. Discharges with Z_{eff}=1-3 are attained without titanium gettering. Lower density and/or higher current discharges are characterized by a large influx of nickel impurity. During some conditions, impurity accumulations near the center are observed.

keywords: Doublet III tokamak, Impurity, Titanium gettering, Nickel, Oxygen, Inconel wall

---

* On leave from Toshiba Electric Co.

** On leave from Mitsubishi Atomic Power Industry

*** General Atomic Co., U.S.A.

This work was done under a cooperative agreement between the United States Department of Energy and the Japan Atomic Energy Research Institute
USDOE Contract No. DE-AT03-80ET51019

インコネルの壁とリミターを用いたDoublet Ⅲ装置におけるD型放電の不純物－チタン蒸着の有無－（タブレットⅢ実験報告・5）

日本原子力研究所東海研究所大型トカマク開発部
藤沢　登・永見正幸・横溝英明・嶋田道也
木島　滋・関　省吾・菅原　享*・小原祥裕
伊尾木公裕**・G.L. Jahns***・N.H. Brooks***
R. Groebner***・狐崎晶雄

（1980年10月16日受理）

Doublet Ⅲ装置のD型放電のパラメータは最大電流1.0 MA，最大密度$1.0\times10^{14}cm^{-3}$，非円型度1.0 － 1.6である。主な不純物は，酸素とニッケルである。ニッケルは壁材であるインコネルの主成分である。チタンゲッターなしでZeff ＝ 1 － 3の放電が得られた。低密度・高電流の領域では，ニッケルの流出が大きい。ある条件のもとでは，不純物が中心に集中する。

* 外来研究員；東京芝浦電気（株）
** 外来研究員；三菱原子力工業（株）
*** General Atomic Company，U.S.A.

Contents

目　　次

1. INTRODUCTION

Experimental study of dee-shaped plasmas in the Doublet III device started in September 1979 [1]. The objective of the Joule heating experiment was to obtain and assess stable discharges which could be applied to the high power neutral beam injection. In concrete terms, the first objective was to produce stable dee-shaped plasmas with high density and high current. The second was to prepare boundary conditions which were able to withstand high power input into the boundary without the release of impurities from limiters and walls.

Dee-shaped plasmas in Doublet III are produced in the upper half of the vacuum chamber. The maximum discharge current is over 1 MA and its Joule input is more than 1 MW. Only Joule input power corresponds to a high neutral beam power in medium-sized tokamak devices. Therefore, it is of great interest and importance to determine whether impurities from the Inconel wall and limiters are permissible or not in discharges with a Joule input power level of 1 MW, and to evaluate whether titanium gettering is indispensable for discharges with a high input power. Furthermore, this data would be of help in judging the most desirable boundary condition for forthcoming neutral beam heating experiments.

To date, stable dee-shaped plasmas with elongations of 1.0 - 1.6 have been obtained. A maximum discharge current of 1.0 MA has been successfully attained and a maximum average density of nearly 1.0×10^{14} cm^{-3} has been achieved [2].

This report aims at accurately describing the impurity status of dee-shaped plasmas with Inconel wall and limiters, both with and without titanium gettering. In the next section, experimental conditions are presented. Experimental results before and after titanium gettering are reported in sections II and III, where the impurity influx is particularly emphasized. In section V, the impurity accumulation near the plasma center, which changes the current profile severely, is discussed. Lastly, we discuss the status of impurities in dee-shaped discharges.

2. EXPERIMENTAL CONDITIONS

Dee-shaped plasmas are produced in the upper lobe of the Doublet III vacuum chamber as shown in Fig. 1. The vacuum chamber and limiters are made of Inconel. the dee-shaped plasmas are limited by the primary limiter and back-up limiters. The primary limiter is installed on the outer wall with the distance between the primary limiter surface and the wall surface 5 cm at the narrowest position. Three back-up limiters are located as shown in Fig. 2. The back-up limiters are placed azimuthally along the length of the vacuum chamber, and project 3 cm beyond the wall surface.

The diagnostic status is also shown in Fig. 2. Diagnostics affording information on the impurity assessment are: a VUV monochromator, which covers the range of the wavelength in 300 - 10 Å; a bolometer array which consists of 5 channels observed vertically; a soft X-ray array which has 12 channels and sights plasmas tangetially on the midplane; and a soft X-ray spectrometer which also sights the plasma center tangentially.

In order to suppress light impurities, titanium was gettered on the vacuum chamber surface. Titanium was installed at $\phi = 240°$, as shown in Fig. 2 and evaporated for 5 minutes between discharges. Approximately half the surface of the vacuum chamber is coated.

Configurations of the dee-shaped plasmas are governed by feedback controlled shaping coils around the vacuum chamber [3]. Plasma parameters obtained are listed in Table 1. Time evolutions of a typical discharge without titanium gettering are shown in Fig. 3. The discharge current abruptly rises to 0.3 MA in a few msec due to the large electric field. During the initial period of around 0.1 s the discharge is not entirely stable, and the signals of the soft X-ray array repeat the abrupt rise and fall. One of the reasons for this phenomenon is thought to be a too rapid rise in the discharge current because the controls are unable to follow the current rise. During this slightly unstable period, a strong plasma-surface interaction such as arcing may occur, and impurities are thought to be introduced into the discharge. This initial phase of discharge into a dee-shaped plasma must be further investigated so as to develop discharges without strong plasma-wall interaction. After this slightly unstable initial period, the discharge current follows the pre-programmed shape.

Hydrogen gas is introduced into the vacuum chamber just before the start of the discharge. After initiation of the discharge, a pre-programmed quantity of gas is supplied through the valve so as to obtain a pre-determined density as shown in Fig. 3. The recycling rate of the working gas appears to be close to one, because, after an interruption of the working gas supuply the density seldom decreases.

3. EXPERIMENTAL RESULTS WITHOUT TITANIUM GETTERING

Discharge cleaning procedures for several days following venting and for a few hours before each experiment suppress light impurities to within a low level. Discharges with high densities have an effective ionic charge of $Z_{eff} \simeq 1.0$. Spectrographic observations of the VUV spectrometer indicate that the dominant impurities are oxygen and nickel. Discharges with low density and/or high current are characterized by metal impurities. The normalized density, $\overline{n}_e \cdot R/B_T$, which is considered to indicate the cleanliness of a vacuum chamber, has attained $\overline{n}_e \cdot R/B_T = 3.4$. This value corresponds to one obtained in medium tokamaks with titanium gettering [4]. The high value of the normalized density is thought to result from the cleanliness of the vacuum chamber and the large size of the machine. The latter is explained by the fact that radiation from light impurities is limited to the area within the plasma boundary; therefore, the larger the machine, the smaller the ratio of the radiated region width to the plasma radius. As a result, a larger machine is of advantage in attaining higher density.

Impurity lines OV (192.9 A), NiXI (148.4A), and NiXXI (95.85A) were studied by a VUV monochrometor for representative light and metal impurities. The behavior of the highly ionized metal impurity NiXXI emitted near the plasma center will be discussed in section V in connection with impurity accumulations near the plasma center. In this section, the impurity intensities OV and NiXI, which are interpreted as being the impurity influx at the plasma boundary, are discussed mainly in relation to various plasma parameters.

Figure 4 shows the density dependence of OV and NiXI. The discharges in Fig. 4 show the K = 1.0 - 1.2 elongation and the discharge current in I_p = 0.4 - 0.5 MA. When the density increases the OV intensity increase is almost directly proportional to the density, while the NiXI intensity

decreases. In particular, the NiXI intensity becomes very high during low density, and the discharge changes into a disruptive one. This disruptive discharge may be caused by the increase in nickel impurity influx. The plasma boundary radiation density ($0.67 \leqq r/a \leqq 1.0$) measured with a bolometer array is presented in Fig. 5. The boundary radiation density has a minimum value at $\overline{n}_e = (2\text{-}3) \times 10^{13}$ cm^{-3}, and increases in both low and high densities. Figures 4 and 5 suggest that increase in boundary radiation density in high and low density regions are caused by an increased influx of nickel and oxygen impurities.

The behavior of the OV and NiXI intensities during varying discharge currents are exhibited in Fig. 6. Discharges in Fig. 6 show an elongation of 1.0 - 1.2 and a density of $\sim 3.0 \times 10^{13}$ cm^{-3}. The OV intensity is independent of the current, and the NiXI intensity increases with the increase in discharge current.

The amount of impurity released from limiters and/or walls depends strongly on the plasma parameters at the edge. Figure 7 shows the profile of electron temperatures obtained by a microwave radiometer at the second harmonic of the electron-cyclotron frequency. The measured temperature profiles have ambiguity at the plasma edge, but these profiles obviously indicate that nickel impurity increases with the increase of the electron edge temperature. On the other hand, oxygen impurity seems to be independent of the edge temperature. The OV line intensity depends on electron density. There is no data on density at the plasma edge. It may be that plasma edge density increases with greater mean electron density, and the more enhanced interaction between plasma and surface results in a large release of oxygen impurity. In the case of the density scan shown in Fig. 7 (a), radiation cooling by oxygen impurity decreases the edge temperature and suppresses the release of nickel impurity. In another current scan [Fig. 7 (b)] the larger Joule input heats the edge temperature and multiplies the influx of the nickel impurity.

Discharges with an elongation of 1.5 have the same effect on density and current as the ones described above for the OV and NiXI intensity. These results from the impurity influx do not contradict those obtained in other tokamaks [5]. The enhanced metal impurity influx is connected to the high edge temperature which is caused by the high power input into the boundary plasma. High current and/or low density discharges turn into disruptive ones.

The VUV spectroscopic instrument is not calibrated. Therefore, the absolute values of impurities are not available. However, the effective ionic charge offers information as to the amount of impurity. Figure 8 shows the effective ionic charge at the plasma center calculated from the central electron temperature and loop voltage. The amount of impurity at the plasma center depends on transport phenomena. In particular, when sawtooth oscillations exist, enhanced outward transport suppresses impurity accumulation near the center and levels the effective ionic charge profile. All the discharges presented in Fig. 8 have sawtooth activities. The effective ionic charge is less than 3.0 and tends to decrease with the increase of electron density. This tendency is the same as in other tokamaks.

The effective ionic charge can also be derived from soft X-ray emissions [6]. Figure 9 shows the profile of integrated soft X-ray intensities measured tangentially with the soft X-ray diode array. The dotted line in Fig. 9 is the hydrogenic bremsstrahlung calculated from the measured temperature profile and the assumed density profile, i.e., parabolic density profile. This discharge has a density of $n_e = 5.0 \times 10^{13}$ cm^{-3}. The ratio of the measured X-ray intensity to the calculated hydrogenic bremsstrahlung, called the enhancement factor, which originates from the impurity, is approximately 3 at the center. The effective ionic charge, which can be estimated from the enhancement factor is almost 1.1. This fact is in good agreement with the Z_{eff} (0) = 1.2 in Fig. 8.

4. CHANGES RESULTING FROM TITANIUM GETTERING

In order to suppress light impurities, in the upper lobe of the vacuum chamber is flushed with titanium. Since there is only one gettering system in the torus, about half the chamber wall is coated, and the primary limiter and the two backup limiters are only partially flushed. The flushing period lasts for 5 min. between discharges with the averaged titanium thickness per evaporation corresponding to $\sim$0.1 monolayers.

Time bahaviors of discharge parameters with high densities are shown in Fig. 10. The difference between discharges with and without titanium gettering is found in the quantity of gas supplied during a discharge. To obtain the same rate in the increase of density as without titanium gettering about 2.0-fold gas is needed in discharges with titanium. Moreover, fairly large quantities of gas have to be supplied in order to hold the density constant. This may cause a change in the recycling rate.

Changes in impurity emission on the OV and NiXI intensities are displayed in Fig. 11. OV has an extreme quantitative reduction and does not increase with increasing density. NiXI also reduces by a factor of two in the high density region, but the increase on NiXI in the lower density region appears in higher densities than the one without titanium gettering.

Changes in radiation density at the plasma boundary as measured by the bolometer array are shown in Fig. 12. There is no increase in high density discharges. This seems to be a result of the suppression of oxygen impurity.

The suppression of light impurities with titanium gettering leads to the attainment of high density discharges. A comparision of maximum densities before and after titanium gettering is exhibited in Fig. 13. A normalized density, $\overline{n}_e \cdot R/B_T \cong 4.5$ is obtained, which means that titanium gettering has obviously been proven.

5. IMPURITY ACCUMULATIONS AT THE PLASMA CENTER

One of the characteristics of a dee-shaped discharge is the accumulation of impurities near the plasma center which severely changes the discharge current profile and increases radiation density in the hot column. This impurity accumulation is observed in discharges with lower densities and higher discharge currents.

Time evolutions of discharge currents, loop voltages, line-averaged electron densities, central electron temperatures, soft X-ray emissions, and NiXXI emissions are shown in Fig. 15 (a). The soft X-ray signals near the plasma center increase up to 0.3 s after an unstable initial period, and then become steady. The soft X-ray signals near the center suddenly start to go down at 0.41 s. During the decreasing of the soft X-ray, strong MHD oscillations are observed on the soft X-ray signals near the center. The profiles of the soft X-ray signals as shown in Fig. 15 (b) are before and after strong MHD activities. NiXXI, which is considered to be emitted near the plasma center, has a time behavior similar to that of the soft X-ray signals. The large soft X-ray emissions are due to nickel impurities near the plasma center. On the other hand, the time evolution of NiXI, which is considered to be an influx from the wall and/or limiters, is constant after the initial 0.1 s.

The profiles of hydrogenic bremsstrahlung for measured temperature and density are plotted in Fig. 15 (b). The enhancement factor is needed in order to adjust the calculation to the observed results. In particular, the soft X-ray signals before MHD activities should use the large enhancement factor, which indicates that impurities accumulate in the plasma center.

The enhancement factors and the effective ionic charges calculated from them are shown in Fig. 16. In this calculation, the main impurity is assumed to be nickel and in the derivation of Z_{eff} value from the enhancement factor we use the calculated table for iron instead of nickel [6]. Figure 16 shows that impurities accumulate in the hot plasma column before MHD activities, and that the accumulation is eliminated by MHD oscillations, which seem to enhance an outward transport of impurities.

The impurity accumulation near the plasma center increases the radiation density from the central region, $0 \leqq r/a \leqq 0.25$. Figure 17 (a) and (b) shows that the central radiation density depends on the soft X-ray intensity. The radiation from the central region is due to the nickel impurity.

6. DISCUSSION

The dominant impurities before titanium gettering are oxygen and nickel, as mentioned previously. Moreover, when the density increases, the OV intensity and the boundary radiation density increase in approximately direct proportion to the increase in density. In discharges with titanium gettering, the OV intensity is remarkably reduced, and the boundary radiation density and OV intensity do not increase with high density. Figure 18 presents the relation between OV intensity and boundary radiation density with and without titanium gettering. This figure suggests that boundary radiation due to oxygen impurity is dominant in high density discharges without titanium, and that low density discharges have large amounts of radiation at the boundary due to nickel impurity. Moreover, in discharges with titanium gettering, radiation due to oxygen impurity seems to occupy (1/2 - 1/3) of the total boundary radiation.

In discharges without titanium gettering, NiXI intensity depends on plasma edge temperature. The NiXI emissions become strong in discharges with lower density and/or high current. Figure 19 shows that NiXI intensity increases with the increase of power $P_J - P_R^T$, which is transferred to the scrape-off plasma and heats it. There is no data on the scrape-off plasma temperature, but Figs. 7 and 19 suggest that nickel impurity influx increases with rising scrape-off plasma temperature. This is not in contradiction with the fact that the cause for nickel impurity release from the wall and/or limiters is sputtering by hydrogen and oxygen, as well as self-sputtering. When Joule input power and/or neutral beam heating power becomes greater, input power into the scrape-off plasma is a great deal more than 1 MW. During this state, the vacuum wall and Inconel limieters are not usable, because sputtering by the wall and limiters becomes very severe and the multiplied influx of metal disrupts the discharge.

No increase in boundary radiation density is observed during high density discharges with titanium gettering. This results from the reduction of oxygen impurity release from the wall and limiters. This suppression of radiation density results in the increase of input power into the scrape-off plasma, and in some conditions of high current discharges, over 0.5 MW power is transferred to the scrape-off plasma. However, a severe increase in the release of Ni impurity was not observed, and high boundary plasma temperatures similar to those observed in discharges without titanium gettering were not always observed. One of the explanations for the cooling of the plasma boundary is the increasing gas supply during discharges. This is a result of the fact that titanium flushing decreases the recycling of hydrogen gas, which then causes an increased need in the hydrogen gas supply greater by a factor of 2.0 than without titantium gettering. However, the increased gas supply alone cannot explain the boundary cooling. In any event, the results of discharges with titanium gettering are incomprehensible and further investigation with high power Joule input is necessary.

Promising candidates for boundary conditions permitting large Joule input and high neutral beam power are low Z material first walls or diverter configurations. Carbon limiters with titanium gettered walls were successfully used in PLT for $\sim$0.1 s of neutral beam heating with 2 MW [7]. Longer periods of neutral beam heating should be investigated. Moreover, impurity accumulations such as those observed in discharges with Inconel limiters are feared to occur in discharges with carbon limiters. In order to assess carbon limiters with high power input, experiments with Joule input of more than 1 MW are going to be made with the DIII device in the near future. Recently, Divertor configurations have been stably produced in the DIII device. The small amount of impurities in the diverted discharges is an encouraging result. The details of which are reported in Ref. [8].

7. CONCLUTION

With the production of dee-shaped plasmas in the upper lobe of the Doublet III device the initial objectives of the Joule heating experiments have been reached. A maximum current of 1.0 MA, maximum mean density of 1.0 x 10^{13} cm^{-3}, and elongation of 1.0 - 1.6 have been achieved. The following conclusive results were obtained concerning the impurity status of discharges with Inconel wall and limiters, both with and without titanium gettering.

Discharges with Z_{eff} = 1 - 3 were obtained without titanium gettering by means of effective discharge cleaning. The dominant impurities were oxygen and nickel. Boundary radiation density increased in both the high and low density regions, respectively.

The accumulation of impurities has been observed near the plasma center. Highly ionized nickel impurities increase near the central region while at the same time there is also an increase in central radiation density. This accumulation is eliminated by the large amount of MDH activity observed near the plasma center, which enhances outward particle transport.

Titanium gettering suppresses the influx of oxygen impurity. The boundary radiation density does not increase in high density discharges. This results in a 34% improvement of the maximum normalized density. There is some incomprehensibility in discharges with titanium gettering. Further investigation of discharges with high Joule power input is needed in the light of the impurity assessment.

ACKNOWLEGEMENT

The authors are grateful to Dr. T. Ohkawa and their many co-workers GAC Doublet-III. The continuing encouragement of Dr. Mori and JAERI staff members in Japan is gratefully acknowledged.

REFERENCES

[1] A. Kitsunezaki, S. Konoshima, M. Nagami, S. Seki, M. Shimada, H. Yokomizo and DIII Group; Bull. Am. Phys. Soc. 24 (1979) 1096.

[2] JAERI D-III Group; to be submitted in Nuclear Fusion.

[3] T. Ohkawa; in Controlled Fusion and Plasma Physics (9th Europ. Conf., Oxford).

[4] S. Konoshima, N. Fujisawa, Y. Gomay, K. Uehara, et al.; Nuclear Materials 76 & 77 (1978) 452.

[5] Y. Shimomura and H. Maeda; Nuclear Materials 76 & 77 (1978) 45.

[6] S. Von Goeler, W. Stodiek, H. Eubank, H. Fishman, S. Grebenshchikov and E. Hinov; Nuclear Fusion 15 (1975) 301.

[7] H. Eubank, R. J. Goldston, V. Arunasalam, M. Bitter, K. Bol, et al.; in Plasma Physics and Controlled Nulcear Fusion Research (Proc. 7th Conf., Innsbruck, 1978) Vol. I, 167.

[8] M. Nagami, et al.; to be submitted in Nuclear Fusion.

Figure Captions

Fig. 1 Upper half cross-section of Doublet III device

Fig. 2 Upper view of DIII device and diagnostics

Fig. 3 Discharge with elongation 1.2. I_p: discharge current, V_L: loop voltage, Teo: central Electron Temperature determined from biharmonics electron cyclotron emission, $\overline{n_e}$: horizontal line-averaged density, GAS: hydrogen gas supply during a discharge, SXR: soft X-ray emission detected by a tangential PIN-diode array.

Fig. 4 Dependence of OV and NiXI intensities on the line-averaged density. Discharge currents are 0.4 and 0.5 MA for 1.0 (∇,o) and 1.2 (Δ,□) elongations, respectively.

Fig. 5 Plasma boundary radiation density ($0.67 \leqq r/a \leqq 1.0$) versus line-averaged density. Radiation densities are determined by 5 channel bolometer array. Discharges with currents of 0.4 - 0.5 MA and elongation 1.0 - 1.2.

Fig. 6 Dependende of OV and NiXI intensities on the discharge current. Discharges have a line-averaged density of 3.0×10^{13} cm and elongation of 1.0 (O,∇) and 1.2 (□,Δ).

Fig. 7 Electron temperature profiles determined by biharmonics electron cyclotron emission. Elongation is 1.0. (a) The discharge current is 0.4 MA (b) The line-averaged density is 3.0×10^{13} cm^{-3}.

Fig. 8 Central effective ionic charge derived from central electron temperature and loop voltage assuming that central safety factor is 1.0. Saw-tooth oscillations are observed in all discharges.

Fig. 9 Soft X-ray emission profile (O) from 10 channel PIN-diode array. Broken line presents pure hydrogenic bremsstrahlung calculated from the measured temperature profile and the assumed parabolic density profile. Solid line is the best fitting bremsstrahlung including enhancement factor which shows 3.0 and 35 at r = 0 and 30 cm, respectively. Discharges are current of 0.6 MA, density of 5.0×10^{13} cm^{-3}, elongation of 1.5. The central enhancement factor indicates that the central ionic effective charge is less than 1.1.

Fig. 10 High density discharge with titanium gettering. Discharge current: I_p, loop voltage: V_L, central electron temperature: T_{eo}, line-averaged density: $\bar{n}_e$, supplied hydrogen gas, soft X-ray emission.

Fig. 11 Density dependence of OV (o,●) and NiXI (△,▲); intensities with (white) and without (black) titanium gettering. Discharge current is 0.5 MA and elongation is 1.2.

Fig. 12 Plasma boundary radiation density ($0.67 \leqq r/a \leqq 1.0$) versus the line-averaged density with (black) and without (white) titanium gettering. Discharge currents are 0.4 - 0.5 MA and elongations are 1.0 - 1.2.

Fig. 13 Stable maximum density versus toroidal field with (O) and without (△) titanium gettering. The line-averaged density is horizontal one, and q_a is 3.7

Fig. 14 Central effective ionic charge with (●) and without (o) titanium gettering, calculated from central electron temperature and loop voltage assuming that central safety factor is 1.0. Saw-tooth oscillations are observed on all discharges.

Fig. 15 Time evolution of plasma parameter and soft X-ray emission profile before (o) and after (Δ) mhd oscillation. Dotted line is pure bremsstrahlung calculated from the measured temperature profile and the assumed parabolic density profile (before mhd activity). Solid and broken lines are the best fitting calculated ones including the enhancement factor before and after the mhd activities, respectively.

Fig. 16 Enhancement factors (ζ) and effective ionic charges (Z_{eff}) of the discharge in Fig. 15. Suffixes A and B present after and before the mhd activity.

Fig. 17 Line-integrated soft X-ray emission through plasma center and central radiation power density ($0 \leqq r/a \leqq 0.33$).

Fig. 18 Relation between boundary radiation power density ($0.67 \leqq r/a \leqq 1.0$) and OV intensity with and without titanium gettering.

Fig. 19 Relation between NiXI intensity and input power into scrape-off plasma, ($P_{IN} - P_R$). P_{IN} is Joule input power and P_R is total radiation power.

Table 1

DEE-SHAPED PLASMA PARAMETERS

Discharge current	$I_p < 1.0$ MA
Loop voltage	$V_L > 1.0$V
Mean line density	$n_e < 1.0 \times 10^{14}$ cm^{-3}
Central electron temperature	$T_{eo} < 1.5$ keV
Effective ionic charge	$Z_{eff} > 1.0$
Electron energy confinement time	$\tau_E^e < 50$ ms
Toroidal field	$B_T < 24$ kG
Gas	Hydrogen
Elongation	$\kappa < 1.6$
Plasma major radius	R = 140 - 143 cm
Plasma minor radius	a = 43 - 45 cm

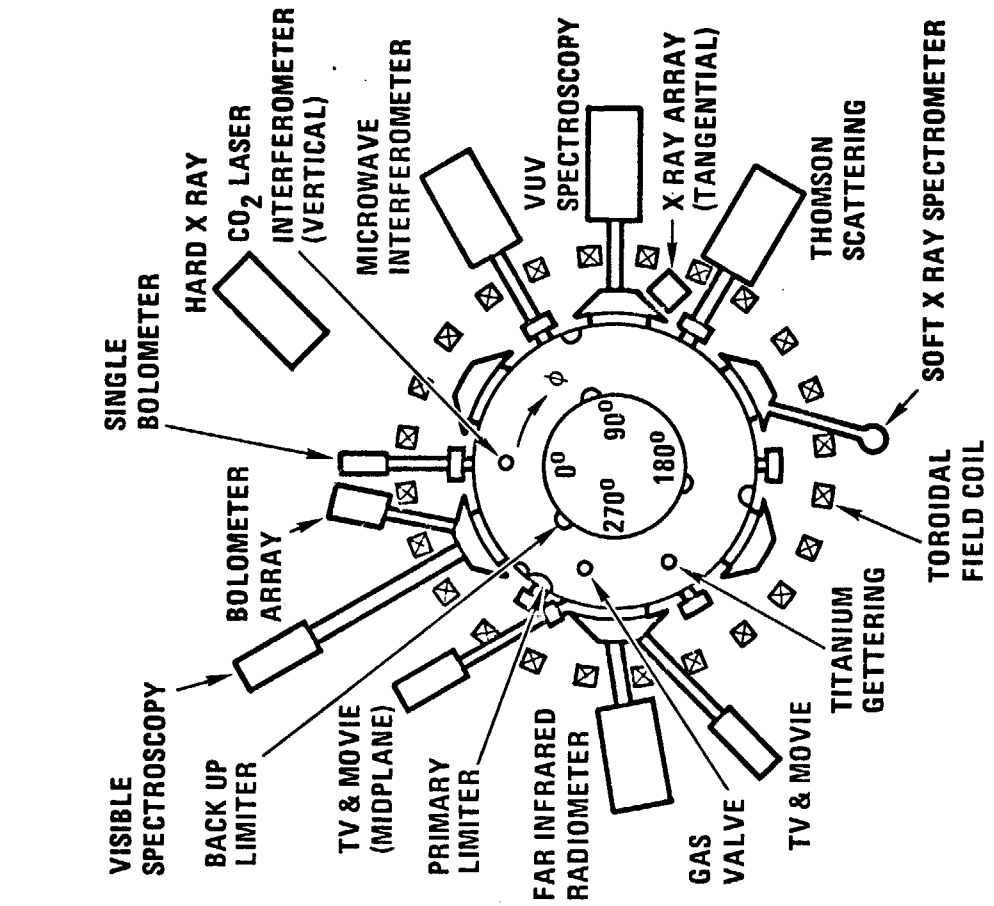

Fig. 2 Upper view of DIII device and diagnostics

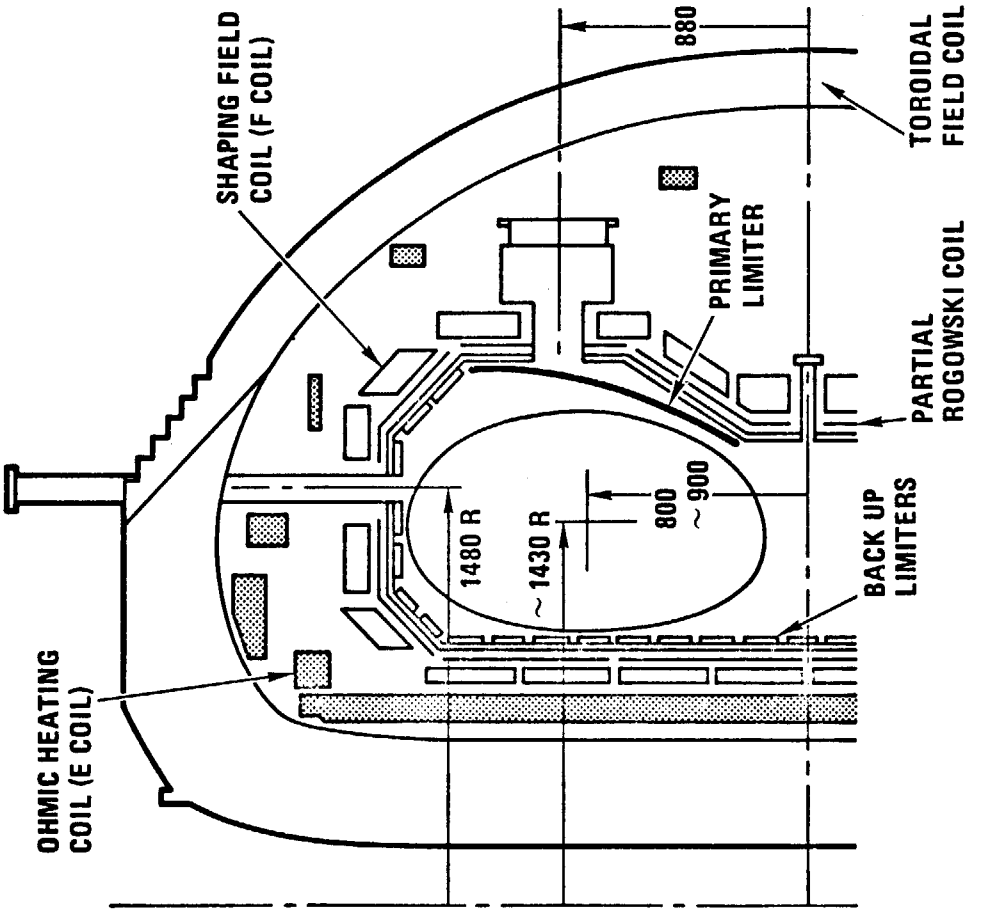

Fig. 1 Upper half cross-section of Doublet III device

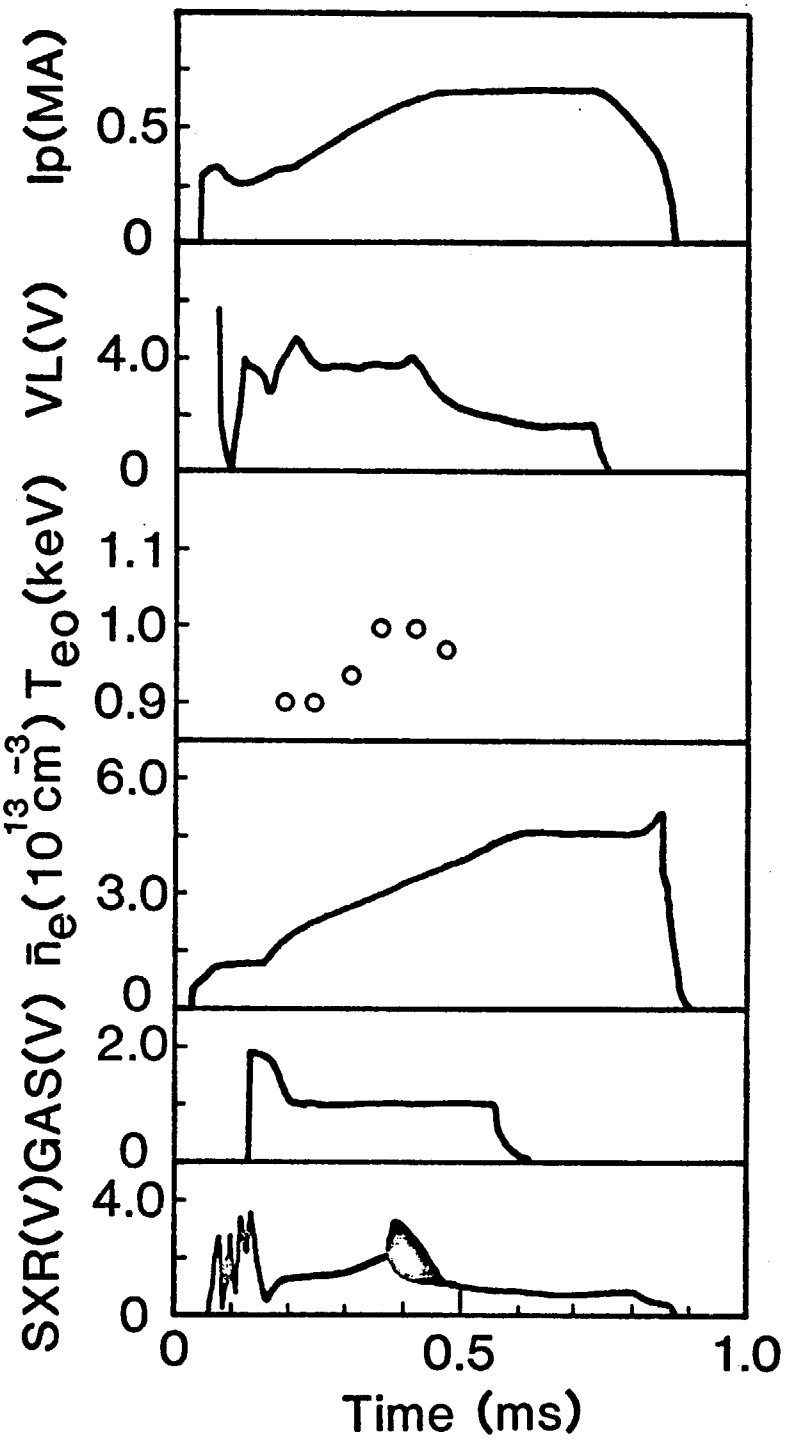

Fig. 3 Discharge with elongation 1.2. I_p: discharge current, V_L: loop voltage, Teo: central Electron Temperature determined from biharmonics electron cyclotron emission, $\overline{n_e}$: horizontal line-averaged density, GAS: hydrogen gas supply during a discharge, SXR: soft X-ray emission detected by a tangential PIN-diode array.

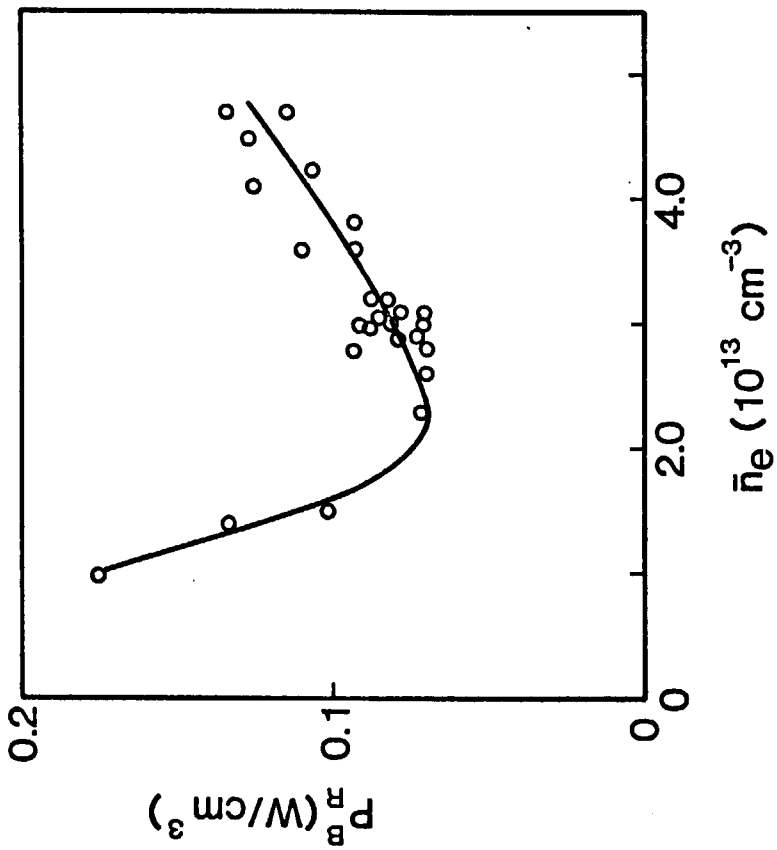

Fig. 5

Plasma boundary radiation density ($0.67 \leqq r/a \leqq 1.0$) versus line-averaged density. Radiation densities are determined by 5 channel bolometer array. Discharges with currents of 0.4 - 0.5 MA and elongation 1.0 - 1.2.

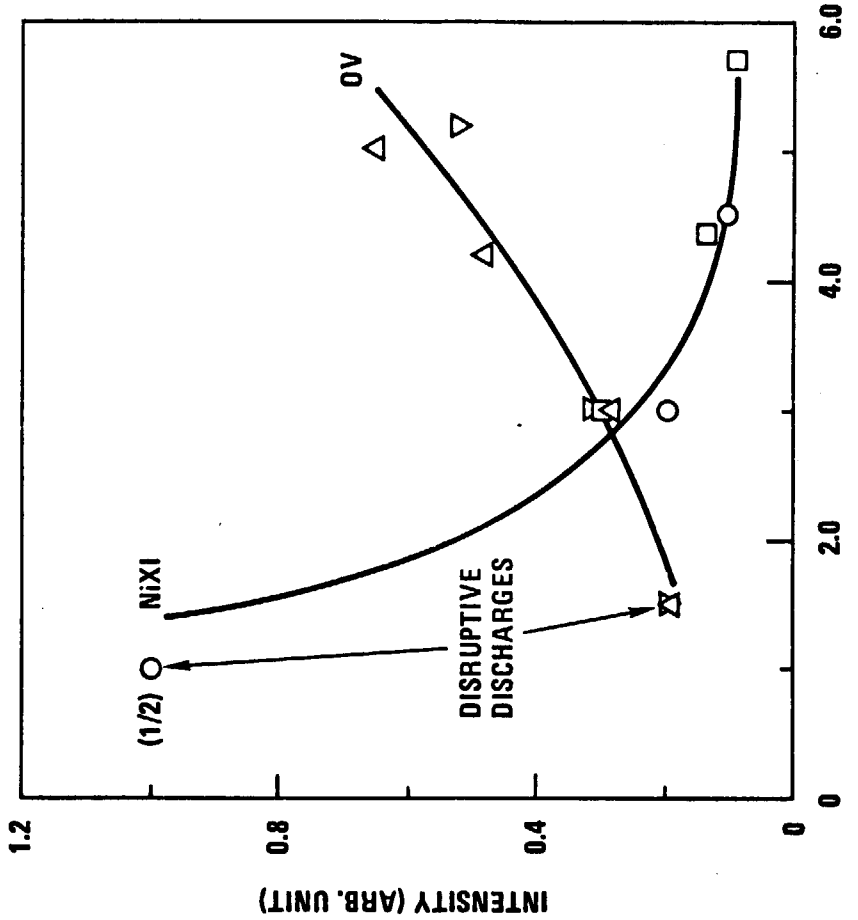

Fig. 4

Dependence of OV and NiXI intensities on the line-averaged density. Discharge currents are 0.4 and 0.5 MA for 1.0 (▽,○) and 1.2 (△,□) elongations, respectively.

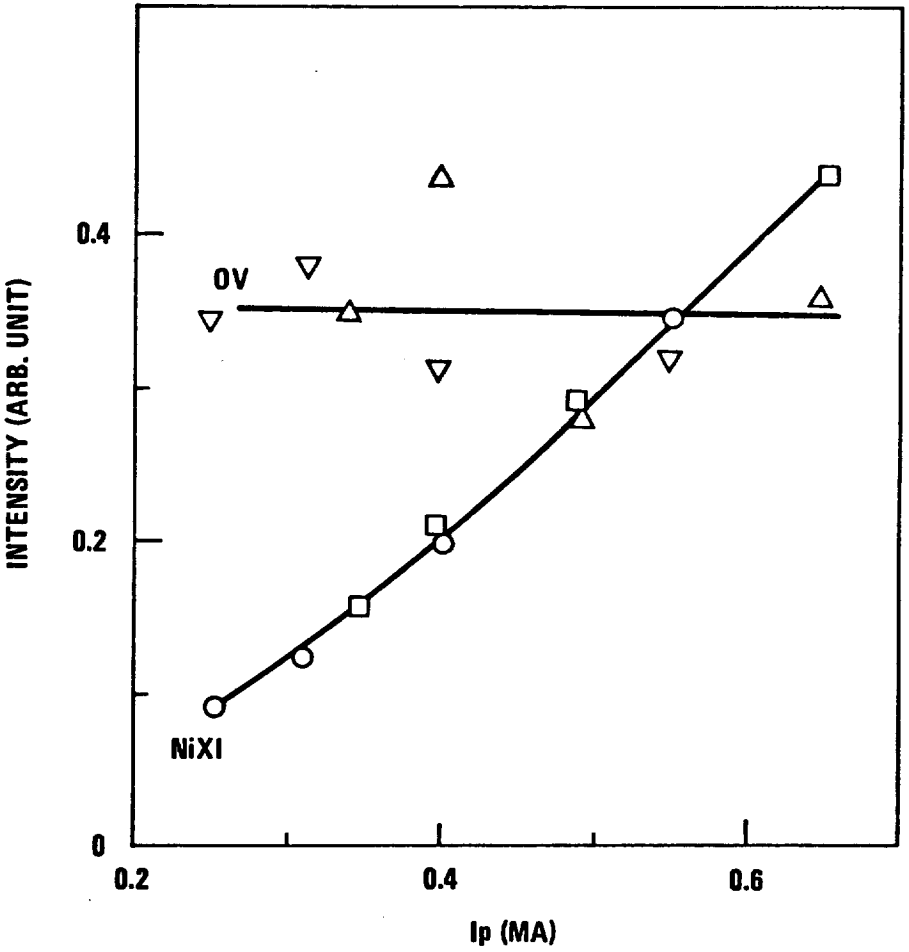

Fig. 6

Dependende of OV and NiXI intensities on the discharge current. Discharges have a line-averaged density of 3.0×10^{13} cm and elongation of 1.0 (O,∇) and 1.2 (□,Δ).

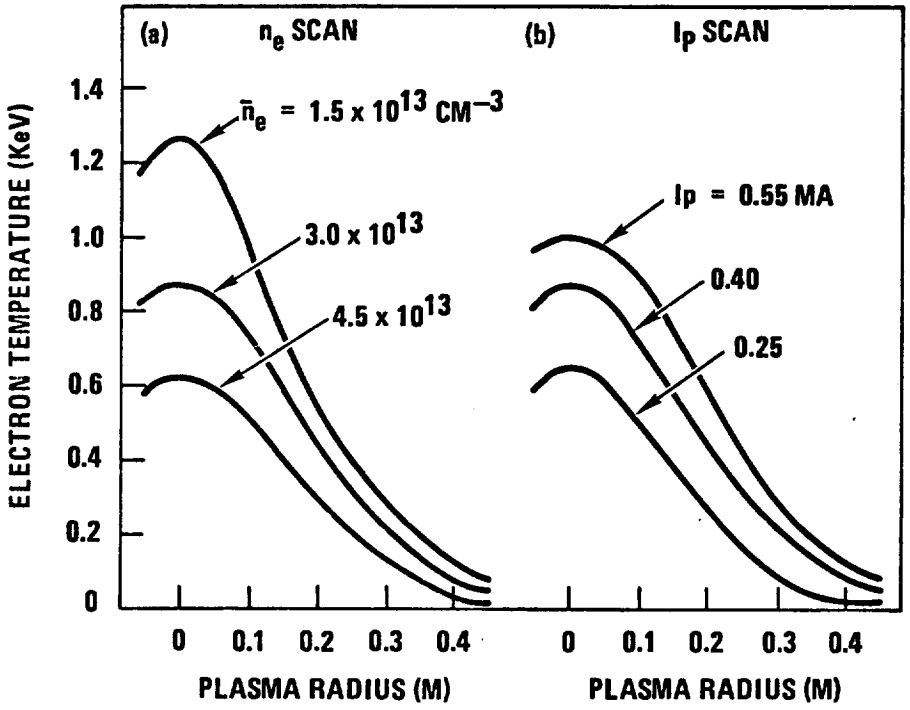

Fig. 7

Electron temperature profiles determined by biharmonics electron cyclotron emission. Elongation is 1.0. (a) The discharge current is 0.4 MA (b) The line-averaged density is 3.0×10^{13} cm^{-3}.

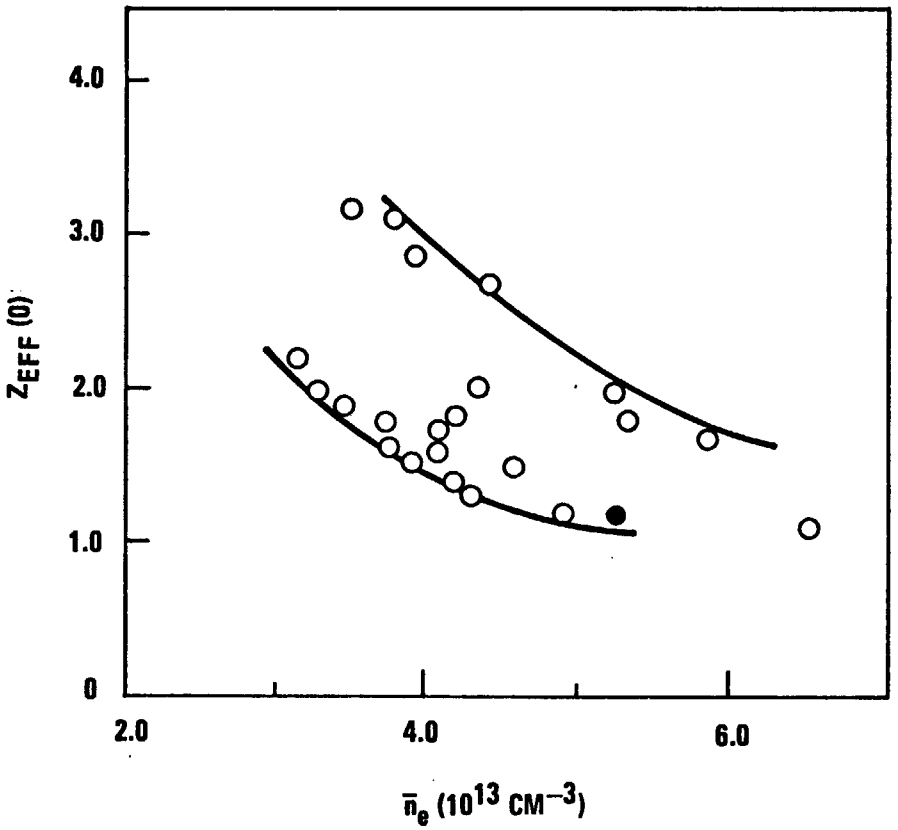

Fig. 8 Central effective ionic charge derived from central electron temperature and loop voltage assuming that central safety factor is 1.0. Saw-tooth oscillations are observed in all discharges.

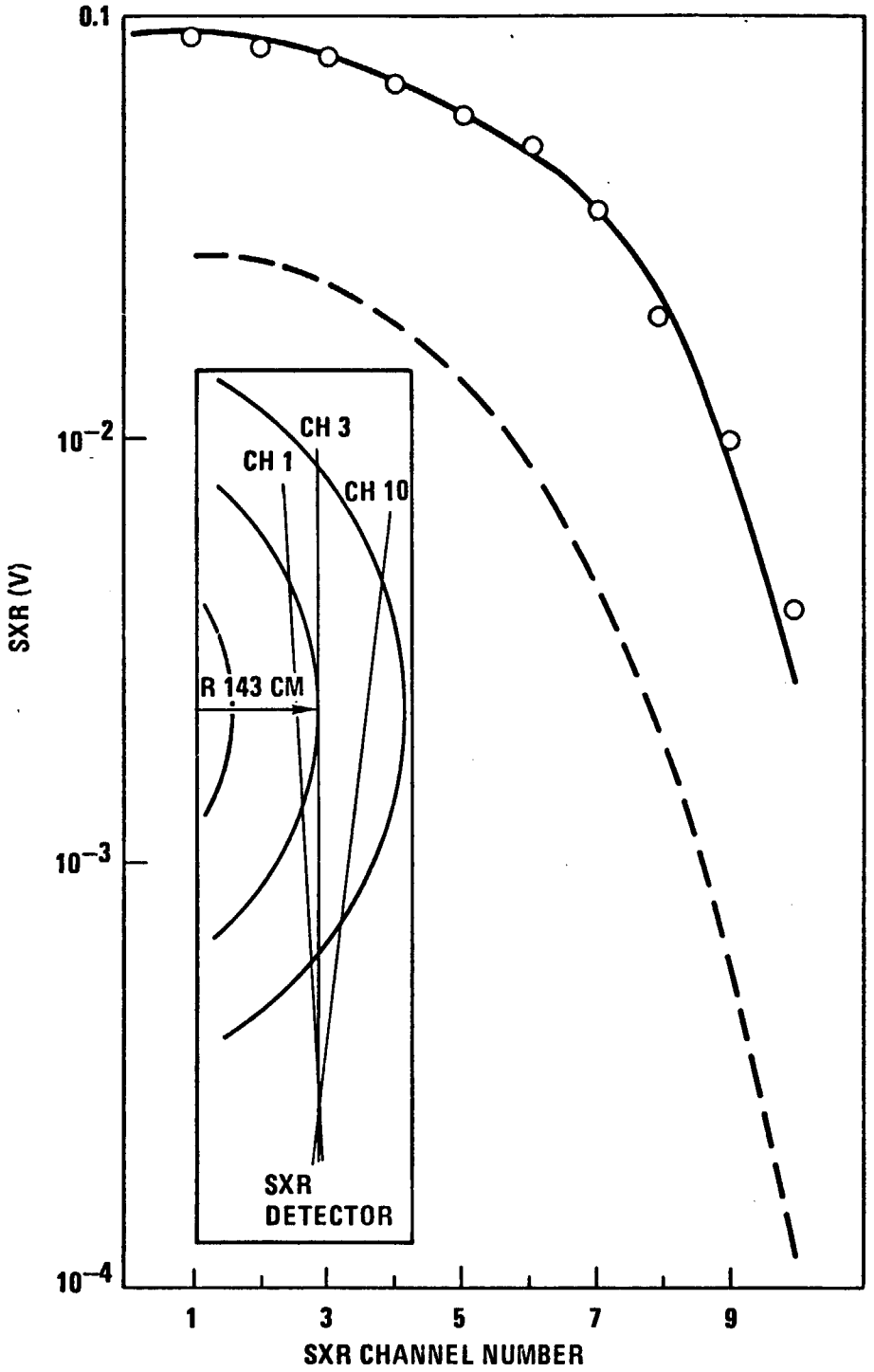

Fig. 9 Soft X-ray emission profile (0) from 10 channel PIN-diode array. Broken line presents pure hydrogenic bremsstrahlung calculated from the measured temperature profile and the assumed parabolic density profile. Solid line is the best fitting bremsstrahlung including enhancement factor which shows 3.0 and 35 at r = 0 and 30 cm, respectively. Discharges are current of 0.6 MA, density of 5.0×10^{13} cm^{-3}, elongation of 1.5. The central enhancement factor indicates that the central ionic effective charge is less than 1.1.

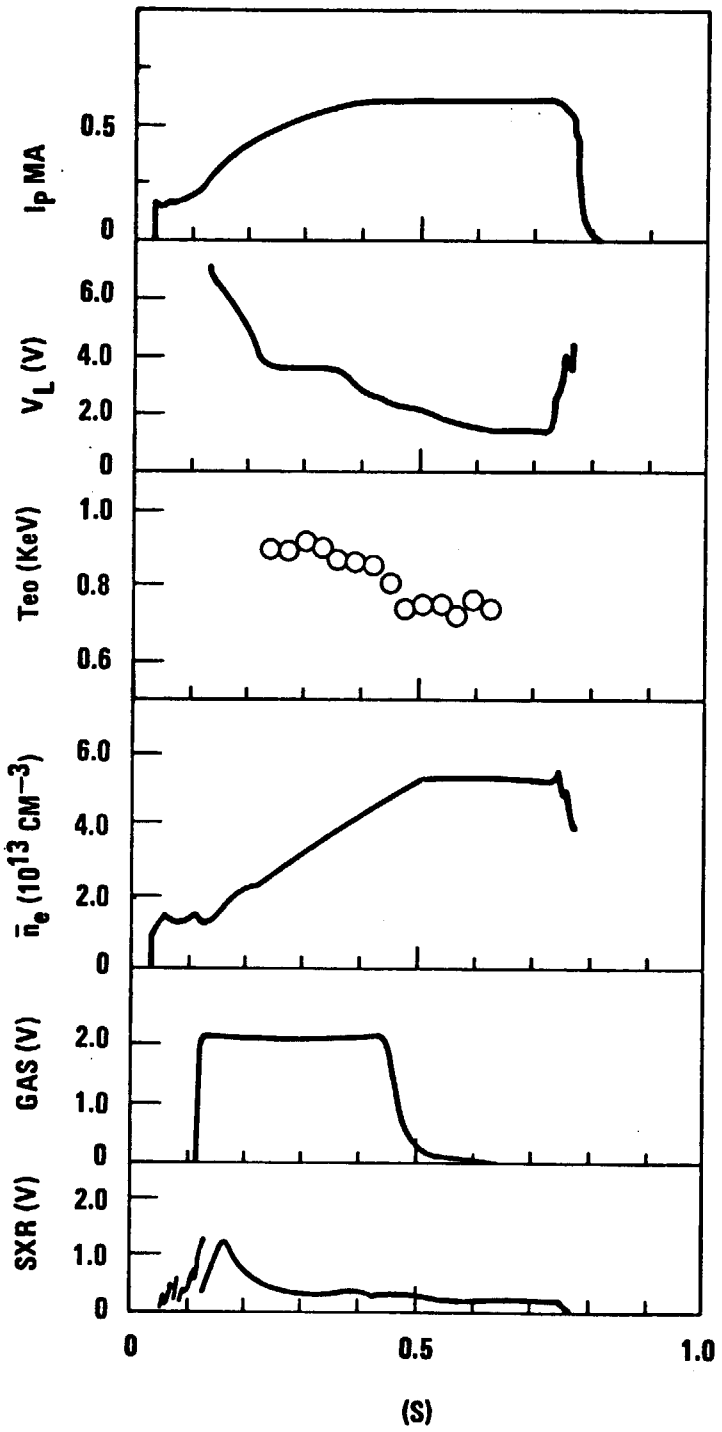

Fig. 10 High density discharge with titanium gettering. Discharge current: I_p, loop voltage: V_L, central electron temperature: T_{eo}, line-averaged density: $\bar{n}_e$, supplied hydrogen gas, soft X-ray emission.

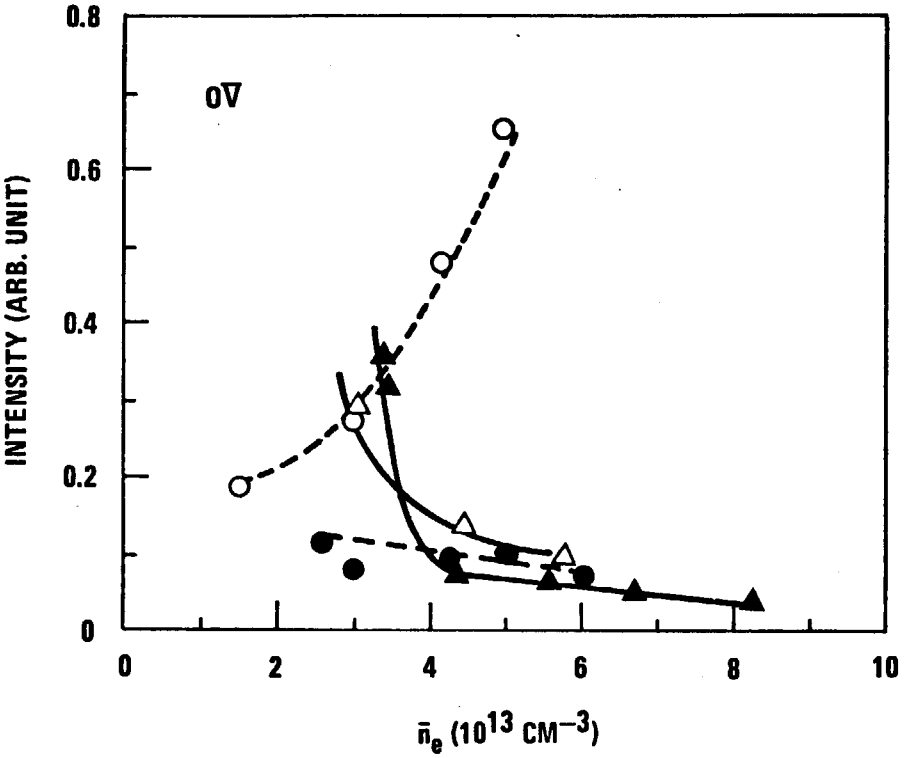

Fig. 11

Density dependence of OV (o,•) and NiXI (Δ, ▲); intensities with (white) and without (black) titanium gettering. Discharge current is 0.5 MA and elongation is 1.2.

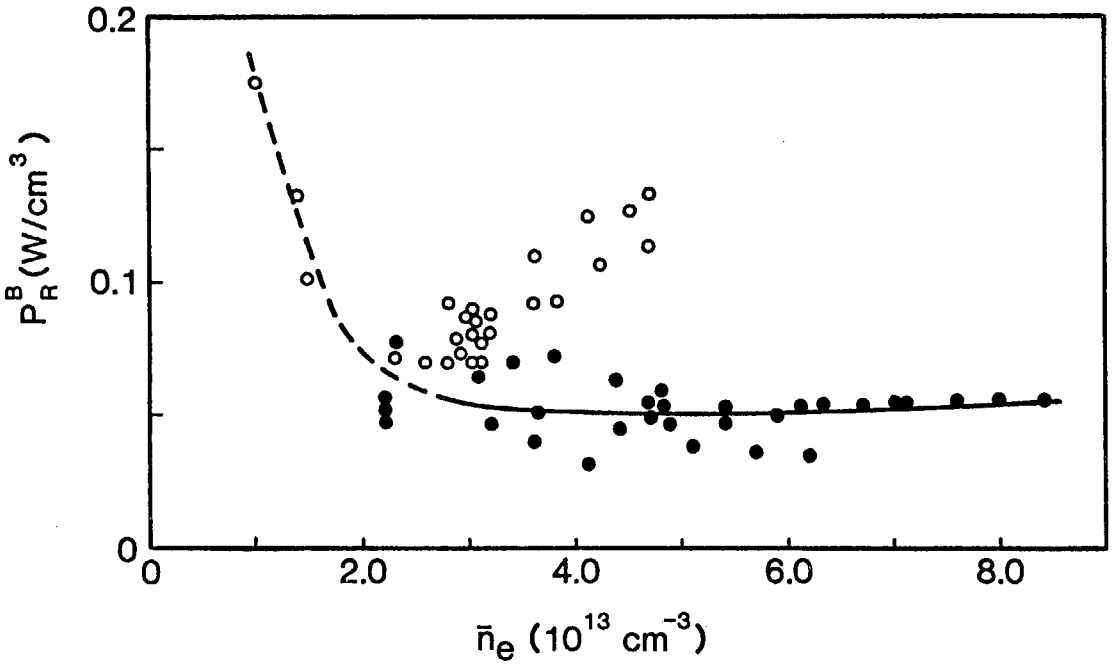

Fig. 12 Plasma boundary radiation density ($0.67 \leqq r/a \leqq 1.0$) versus the line-averaged density with (black) and without (white) titanium gettering. Discharge currents are 0.4 - 0.5 MA and elongations are 1.0 - 1.2.

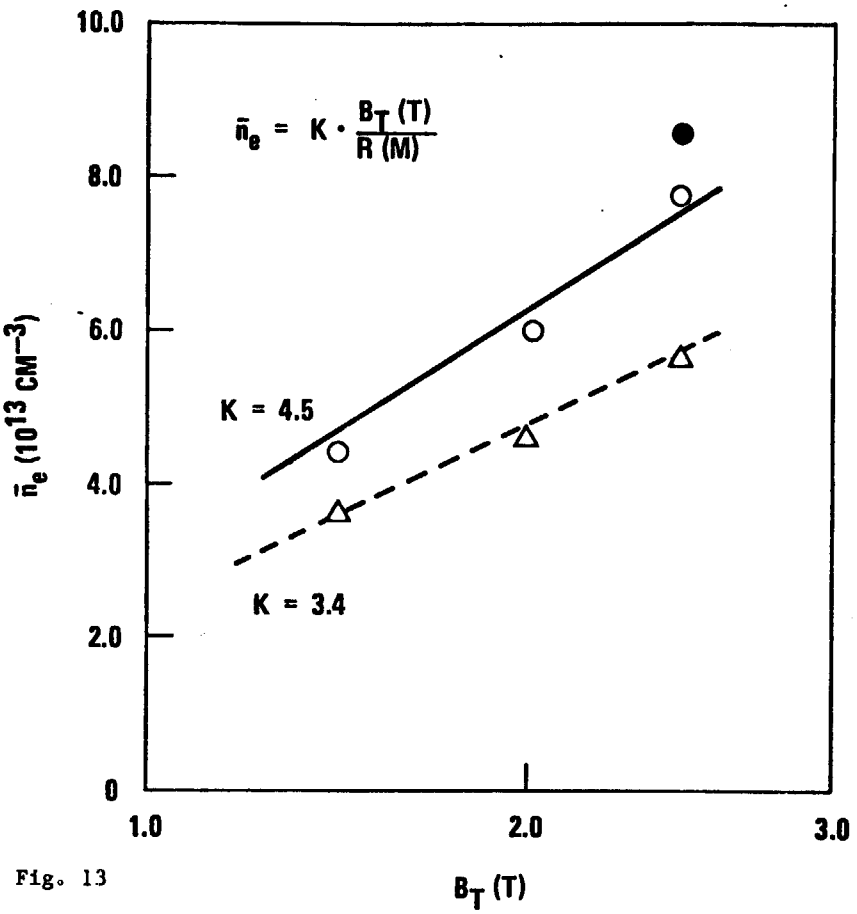

Fig. 13

Stable maximum density versus toroidal field with (O) and without (Δ) titanium gettering. The line-averaged density is horizontal one, and q_a is 3.7

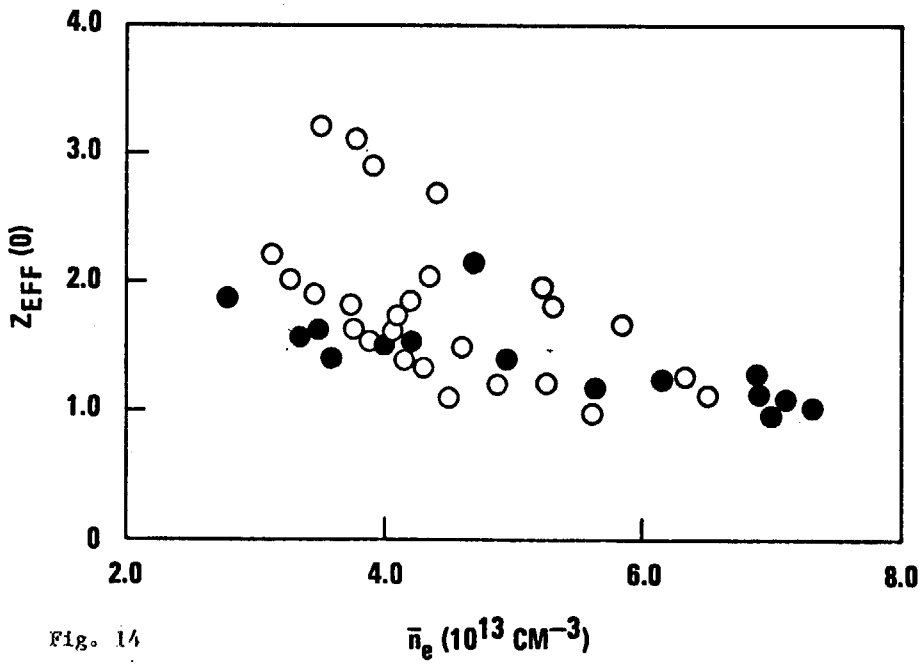

Fig. 14

Central effective ionic charge with (•) and without (o) titanium gettering, calculated from central electron temperature and loop voltage assuming that central safety factor is 1.0. Saw-tooth oscillations are observed on all discharges.

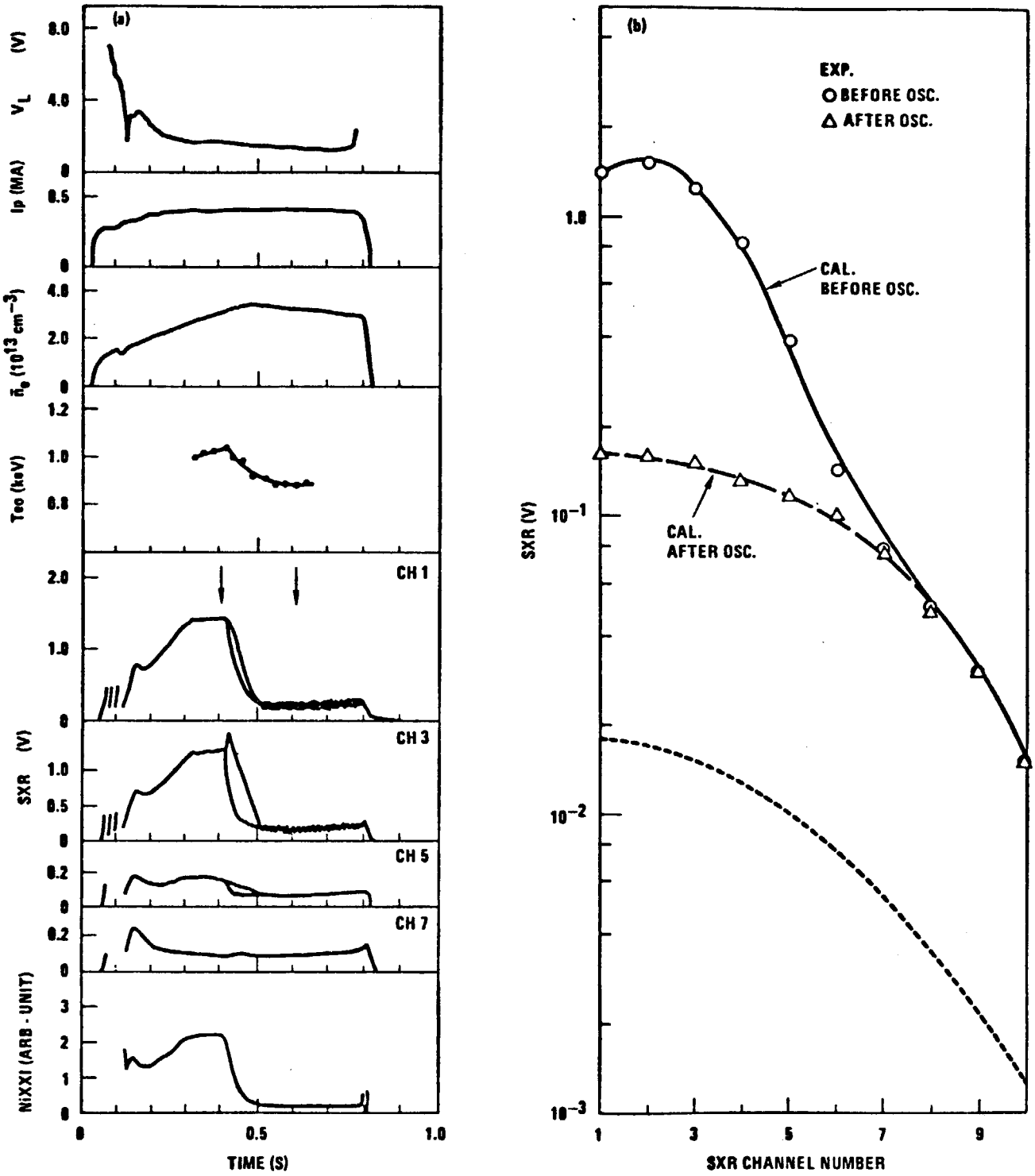

Fig. 15 Time evolution of plasma parameter and soft X-ray emission profile before (o) and after (Δ) mhd oscillation. Dotted line is pure bremsstrahlung calculated from the measured temperature profile and the assumed parabolic density profile (before mhd activity). Solid and broken lines are the best fitting calculated ones including the enhancement factor before and after the mhd activities, respectively.

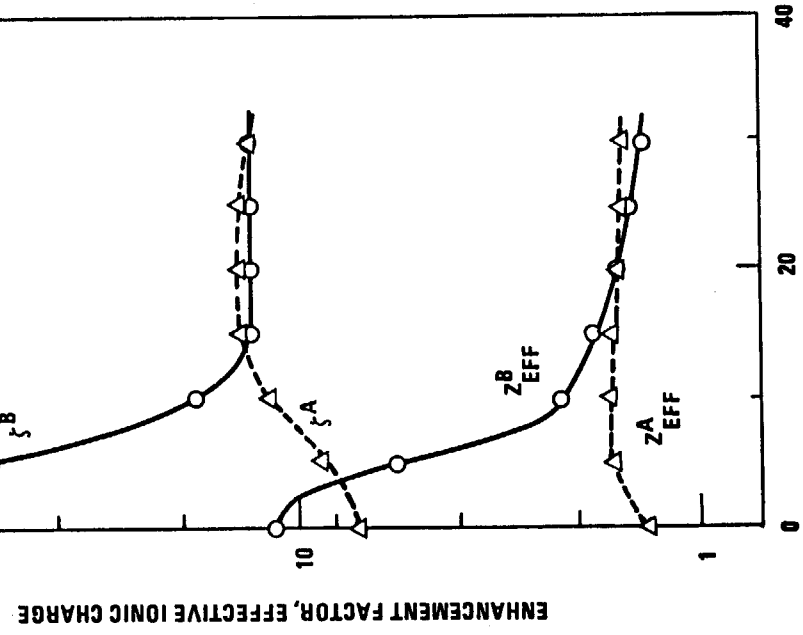

Fig. 16
Enhancement factors (ζ) and effective ionic charges (Z_{eff}) of the discharge in Fig. 15. Suffixes A and B present after and before the mhd activity.

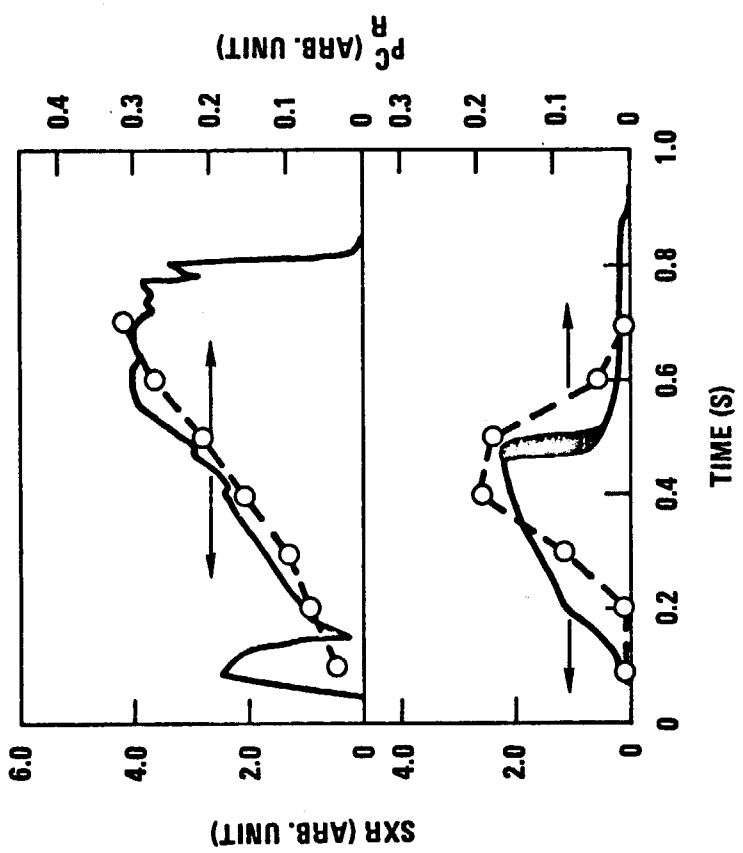

Fig. 17
Line-integrated soft X-ray emission through plasma center and central radiation power density ($0 \leqq r/a \leqq 0.33$).

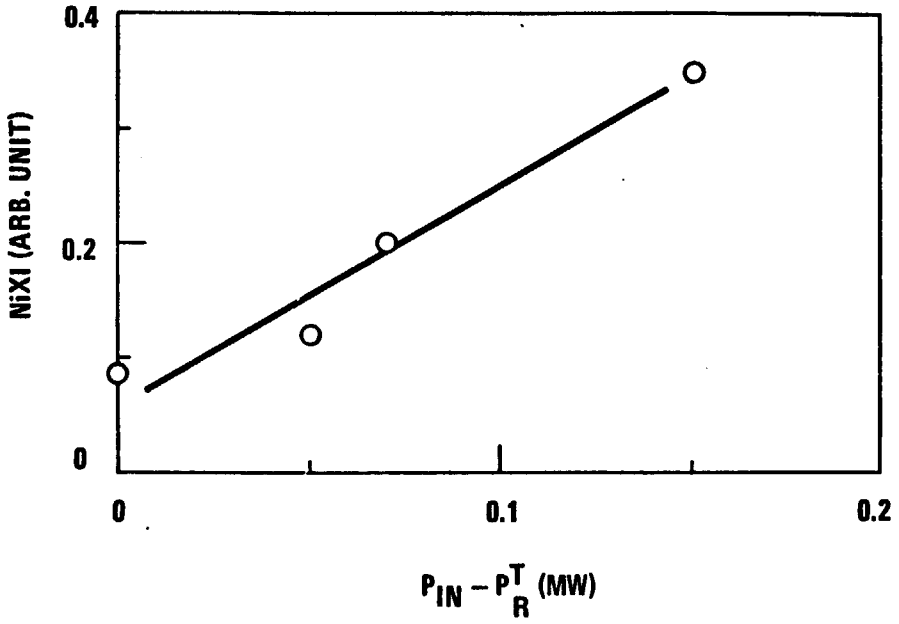

Fig. 18

Relation between boundary radiation power density ($0.67 \leqq r/a \leqq 1.0$) and OV intensity with and without titanium gettering.

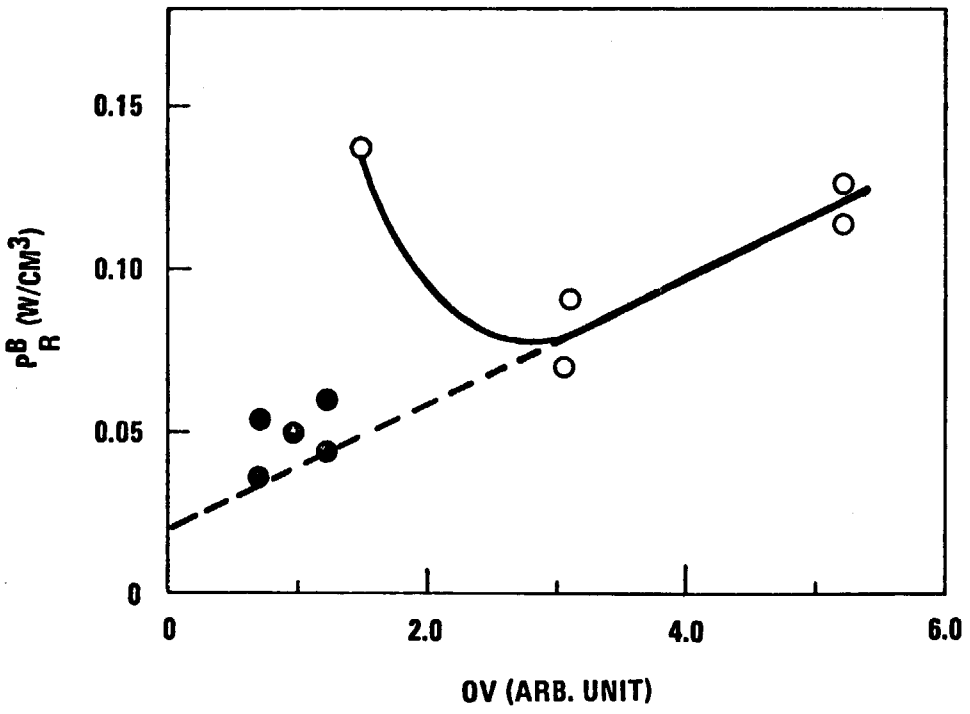

Fig. 19

Relation between NiXI intensity and input power into scrape-off plasma, (P_{IN} - P_R). P_{IN} is Joule input power and P_R is total radiation power.